

CIRCUMFERENTIAL PRESSURE DISTRIBUTIONS IN A MODEL LABYRINTH SEAL

Y. M. M. S. Leong and R. D. Brown
Heriot-Watt University
Riccarton, Edinburgh EH 14 4AS
Scotland

SUMMARY

Leakage flow through labyrinth glands had long been known to affect rotor stability but its effects have been often underestimated. A research programme to isolate and study this cause of instability has been initiated. Circumferential pressure distributions are measured in the labyrinth glands with geometry appropriate to the high pressure labyrinths in large steam turbines. Knowledge of this pressure distribution is essential as it is this unequal pressure field that results in the destabilising force. Parameters that are likely to affect the pressure distributions are incorporated into the test rig. Some preliminary pressure profiles are presented.

INTRODUCTION

Over the last few decades the development of steam turbines and gas turbo compressors has resulted in a steady increase in the energy density of the working fluid. Thus the energy available for various mechanisms leading to unstable motion also increases. The increase in power implies an increase in length of turbine-generator sets as these machines operate at a fixed speed (3000 or 3600 rpm). This makes the machine less rigid and the operational speed often lies above the first and second criticals. High level nonsynchronous vibrations have often been attributed to instability arising from lightly loaded bearings. The light loads instability problem is accentuated by the presence of a large number of bearings supporting a typical rotor with rigid couplings. Operational practice ensures that each bearing takes a load and/or the use of more stable bearing configurations, e.g. lemon-bore. In extreme cases tilting pad bearings may be used. If the instability arises in the bearings then the problem will be eliminated. However, there are other sources of instability which may prove to be significant. Steam whirl associated with differential clearance at the periphery of a blade row has long been suggested as a possible source. The possibility of labyrinth seals inducing instability has not been given the same weight of attention. The destabilising forces were considered by Pollman to be insignificant (ref.1). Furthermore it has been concluded that instability arises if and only if the labyrinths converge, Alford (ref.2); or diverge Spurk (ref.3) which of course led many to conclude as highly unlikely to occur in practice. It is also argued that the pressure in the labyrinths would equalise and hence cannot maintain the unequal pressure field which is essential in producing the lateral forces acting on the rotor.

Recent experience has indicated that the dynamic effects have been underestimated. Based on operational steam turbines, Greathead (ref. 4,5) has brought

to light the influence of the labyrinth sealing glands, in particular at the high pressure end adjacent to the working fluid inlet, on the sub-synchronous response and the instability threshold. The response is strongly load dependent and has a major frequency component greater than half speed. Evidently the resultant destabilising force re-excites the lower criticals. A further interesting observation here was that the replacement of the standard journal bearings with tilting pad journal bearings had detrimental consequences on the response. This indicates that an instability which does not originate from the bearings cannot be eliminated by the use of tilt pad bearings.

NOTATION

p	absolute pressure	n	number of labyrinth stages
p_o	absolute pressure at entry	ϵ	eccentricity ratio
p_n	absolute pressure at exit	r	radius of rotor
q^*	mean axial flow	U	rotor surface velocity
q	axial flowrate per unit circumference	c	circumferential velocity of fluid in gland
μ	flow coefficient	v	axial velocity of fluid
ν	kinematic viscosity	Re	circumferential Reynolds number (= $(U-c)h/2\nu$)
$\Delta\mu_{1,2}$	change of flow coefficient at narrow, widest clearance	Re_a	axial Reynolds number (= $2v\bar{\delta}/\nu$)
ρ	density	Ta	Taylor number (= $Re\sqrt{h/r}$)
R	gas constant	θ	peripheral angle, measured from widest clearance
T	temperature	x	horizontal coordinate (= $r\theta$)
δ	radial clearance	z	axial coordinate
h	height of labyrinth fin		
f	cross-sectional area of gland		
L'	wetted perimeter of gland per unit circumference		
L''	wetted perimeter of rotor per unit circumference		
			Subscripts
		i	i -th gland
		-	mean value

CURRENT STATE OF ART

Reports on labyrinth induced instabilities date back as early as the 1950's (ref.6). A physical explanation of the occurrence of self-excited vibrations through clearance flows at the blade tips and interstage glands was presented by Thomas (ref.7). It is already recognised that these vibrations were very much load dependent. Alford introduced further understanding to the problem in his report on aerodynamic exciting forces on jet turbo compressors and turbines (ref.2). The occurrence of a circumferential variation of static pressure acting on the cylindrical surface of a rotor particularly within labyrinth seals was put forward. The whirl frequency was identified as the fundamental frequency of the rotor and rotor support system whose whirl speed was about 40 to 50 percent rotational speed. The whirl amplitude increases with power output. It is concluded that unequal radial clearances at entry and discharge have significant effect on the excitation. Based on a single chamber labyrinth a stability criteria was arrived at, with converging labyrinth glands being destabilising. This stability criterion was contradicted by Spurk (ref.3) in that diverging labyrinths are destabilising instead. In common with Alford the rotational motion of rotor is neglected in the stability analysis and the reason given for the contradiction is due to the further neglect of circumferential flow within the labyrinth by Alford. Further literature (ref. 8,9) indicates that lateral forces can be produced by parallel clearances when eccentricity exists, with or without the occurrence of spiral flow; and these lateral forces lead to unloading of radial bearings.

Until 1975 approximately comprehensive experimental work on multi-stage labyrinths is non-existent, and at best the destabilising forces are only defined qualitatively. Among the first attempts to analytically quantify these forces in multi-stage labyrinths was by Kostyuk (ref.10). A set of fundamental equations correlating leakage flow, circumferential flow and pressure distribution was arrived at by applying compressible gas dynamics and conservation of energy and momentum. Simplified solution to the equations was forwarded for cases with tilt although the form of solution arrived at predicts no unequal pressure distribution for cases of parallel eccentricity between rotor and labyrinths. The application of Kostyuk's equations were extended by Iwatsubo and Kurohashi et al (ref. 11, 12). Iwatsubo applied a finite difference method on the equations with the spring and damping coefficients of the labyrinths numerically determined. With a simpler approach Kurohashi et al applied an equivalent clearance to take into account of the variable flow coefficient through the annular clearance of the labyrinths to arrive at a pressure distribution and set of stiffness and damping coefficients. No swirl or spiral flow was assumed nor considered. Although some experimental work was performed the published data were found to be rather limited especially on the pressure distributions. Pressure measurements were made at only two opposite locations within a labyrinth chamber hence with the assumption that the pressure peaks at such location.

The experimental work of Benckert and Wachter (ref. 13,14,15) represents the first serious attempt to investigate the leakage flow induced forces on multi-stage labyrinths. It was an extensive experimental programme on labyrinths on a high pressure air rig. Various geometry, number of stages, inlet conditions, eccentricity and realistic peripheral velocity of rotor were catered for. Pressure profiles were indeed obtained on cases with a parallel eccentricity through the labyrinths and swirl has an increased forcing effect on the rotor. However the published results were mainly of integrated forces and only few pressure distributions were published,

pressure distributions with rotor rotation were not presented. As the interest of the authors was towards gas turbo compressors the published work was based on geometry and dimensions not appropriate to steam turbines.

It is this lack of directly applicable experimental results in open literature based on realistic seal geometry with full rotational speeds that necessitates the need for further research. This research programme on labyrinth seals was a natural extension of existing work on rotor dynamics in the Department of Mechanical Engineering at Heriot-Watt University. Work on rotordynamic instability included the effects of high pressure ring seals on turbomachinery vibrations, fluid force induced vibrations, boiler feed pump instability and a general rotor dynamic computer programme evaluating forced response and stability. It is ultimately hoped that the programme would incorporate labyrinth seal forces to extend its range of applicability.

OBJECTIVE

The main objective of the rig is to isolate the labyrinth induced effects from other rotor dynamic effects that can possibly arise. A rotor diameter approximately half that of a typical steam turbine shaft is used. Nevertheless the rotor and labyrinth dimensions should meet the requirement that the flow parameter of Reynolds number and Taylor number are of the same order of magnitude both in the axial and circumferential direction. As it is felt that the rotor peripheral velocity is of importance in the shearing of the leakage flow, a realistic velocity must be attained on the rig, in this case of 100 m/s as in operational steam turbines. Consultation on the above data and seal geometries had been made with United Kingdom based manufacturers and public utilities.

The approach taken is to measure the static pressure distributions in the labyrinth chambers as the flow passes through the labyrinth and to match these measured distributions with theoretical predictions. An alternative method is to attempt to measure overall force and/or stiffness coefficients directly. However the literature has a number of examples where considerable scatter was demonstrated in attempts to measure stiffness and damping coefficients. Moreover circumferential pressure distributions give a better insight into the nature of the problem. It is interesting to know how these pressure distributions are affected by eccentricity, clearance, speed and a host of other parameters. When an adequate match has been achieved between experimental and theoretical circumferential pressures, the required dynamic coefficients can be obtained theoretically. The integrated pressure force for overall perturbed conditions yield the appropriate stiffness and damping coefficients.

DESCRIPTION OF RIG

The experimental rig consists of a main casing enclosing the rotor and labyrinth assembly, figures 1,2,3. The main casing is made up in two sections with the upper section easily removable to enable the labyrinth assembly, especially combination and stepped labyrinths, be built up conveniently. Slots are milled on the casing adjacent to the labyrinth assembly to facilitate the mounting of pressure tappings in the labyrinth. A vertical rotor is mounted on roller ball bearings

within the casing. The top bearing housing is bolted on to the main top cover plate and the bottom bearing housing on the main platform on which the casing is bolted. Drive is by means of a horizontally mounted 8.5 kW variable speed DC motor, with the driving shaft attached to a 1:1 right angle conversion gear box. The rotor is driven by a timing belt from the gear box with the necessary step up in speeds achieved through the pulleys giving speed ranges from 0 to 7600 rpm.

Consistent with the need to isolate other rotor dynamic effects a rigid rotor is used. This eliminates the influence of hydrodynamic bearings as well as making it easy to preset and maintain predetermined eccentricities. Mounting it vertically eliminates the need to consider gravitational effects in the experiments and subsequent theoretical work. Grease lubricated self aligning ball bearings are used at the top to allow for small relative misalignment between the rotor and main casing for tilt investigations. To take the high downwards thrust a matched pair of angular contact ball bearings is used in tandem. The bottom bearings are oil lubricated from nozzles directed on to the cages and races allowing them to be used at the higher speeds. A high pressure thrust compensating dummy piston could have been incorporated into the design but was not as conservation of the available working fluid was a major consideration. In order to achieve the peripheral velocity of 100 m/s, a drum of 240mm in diameter is mounted on to the main shaft to form part of the rotor. The drum is interchangeable and the experiments will involve the use of a plain drum and grooved drum for various labyrinth combinations. The axial length of the drum is 160mm to accommodate the axial length of a complete labyrinth assembly. The main shaft and drum are first balanced individually and finally as a completed assembly to ISO G 1.0 (1 gm-mm per kg rotating mass).

The working fluid is fed into a diffusion box in the main casing. Within the diffusion box deflection vanes and perforated holes spread the flow. From here the flow enters a plenum chamber where the flow is further settled. The working fluid used is compressed air at a gauge pressure of 5.52 bar although higher pressure or higher density compressed gas can easily be adapted for use on the rig. The flow rate through the rig is measured by an annubar. It has four dynamic pressure sensing holes facing the stream, and the dynamic pressure being averaged by means of an interpolating inner tube. A further pressure sensing hole measures the static pressure less the suction pressure which eventually gives a differential pressure representing the mean velocity along the tube. This measured flow rate is compared with the extensively used and tested semi-empirical labyrinth leakage equation of Vermees (ref.16) as well as equation 1. (ref. 10,12). Axial and circumferential Reynolds number and Taylor number of 33×10^3 , 63×10^3 and 17×10^3 respectively can be attained on the rig as compared to typical values of 222×10^3 , $124 \times 10^3 - 216 \times 10^3$ and $14 \times 10^3 - 35 \times 10^3$ respectively on operational United Kingdom steam turbines. Nevertheless one of the main current constraints on the rig is due to the limitations of output from the compressors of the Department. Just prior to entry into the labyrinths the flow enters a set of swirl ring mounted on top of the labyrinth assembly. These rings are interchangeable with vane angles of 45° , 30° , 15° and 0° . These swirl rings can hence pre-induce a spiral flow prior to entry into the labyrinth assembly. As the rotational direction of the rotor can be reversed the case of the pre-swirl in opposite direction to the rotation of the rotor is also possible. The 0° vanes are used as a flow straightener when no pre-swirl is required.

Depending on dimensions, the labyrinth assembly is built up from interlaying individual seal fin and chamber or as in integral individual labyrinth, figures 4,5. This allows interchangeability of seals with different geometry, sizes and

clearance. The current sizes used for straight through labyrinths are 4.064mm (height) x 6.350mm (axial length) and 9.525mm x 9.525mm being the largest size to be used; with clearances of 0.254mm - 0.635mm. Stepped and combination seals of 4.064mm/4.620mm x 6.350mm are also used. Further combination of labyrinth dimensions can be catered for by mere manufacture of the fins required. The number of stages can be altered by removing or adding appropriate individual fins. The current number of stages considered total up to 12 labyrinth chambers, although more can be added. Custom made pressure fittings are mounted on recesses in the individual labyrinth fins to measure static pressure circumferentially at 30° intervals in each and every stage down the labyrinth stack.

The eccentricity of the rotor with respect to the labyrinths can be set at any predetermined location. The labyrinth assembly together with the main casing as a whole is moved laterally across the main table platform, with the rotor and its bearings housings being fixed in its original location. The movement is achieved by means of lateral finely threaded jack screws, with the main casing moving in guide blocks. To minimise the effort required to move the job, four sets of ball bearing thrust pads are brought into play raising the main casing and assembly off the table platform whilst being moved. Lateral adjustable pre-compressed springs are mounted against the casing to eliminate any backlash on such small movements. The eccentricity is checked by means of displacement proximators as well as dial gauges. Other than parallel eccentric movement a relative tilt between the rotor and labyrinths can be set. Here again the rotor is left undisturbed and the main casing with the labyrinth assembly tilted. This is so achieved by raising the main casing off the platform and an angled tilt pad inserted between the main casing and platform.

The experimental parameters are

- (i) seal geometry and types: straight through, stepped and combination labyrinths
- (ii) number of stages
- (iii) relative tilt between labyrinths and rotor
- (iv) flow rate and inlet conditions, including swirl
- (v) eccentricity
- (vi) rotational speed of shaft.

At each setting of these parameters static pressure measurements are taken as the leakage flows through the labyrinths. The current total of 144 pressure distribution measurements of the labyrinth assembly as well as static and dynamic pressure measurements at the inlet and outlet are fed to a bank of mechanical rotary switches. These switches allow 5 pressure lines, on the inlet ports, to be served by 1 pressure transducer at the outlet port of the switches. At each inlet port setting a scan of all the pressure transducers are taken and sequential switching of open inlet ports gives a complete pressure mapping. As static pressure measurements are of interest here this arrangement would be more cost effective than electronics based scanning valves. The working fluid inlet and outlet temperature from the labyrinth assembly are also monitored by thermocouples to validate the theoretical assumption that the two temperatures are constant. The scanning of the pressure transducers as well as thermocouples and proximators are activated via a data transfer unit, giving output in forms of readings on the digital voltmeter and paper tape for final processing on a digital computer.

SUMMARY OF THEORY

Assuming an isothermal process in a multi-stage labyrinth glands and the working fluid to be a perfect gas, Kostyuk (ref.10) derived a set of fundamental equations as follows:

$$P_{i-1}^2 - P_i^2 = \frac{q_i^2 RT}{\mu_i^2 \delta_i^2} \quad (1)$$

$$\frac{\partial \rho_i}{\partial t} + \frac{\partial(\rho_i c_i)}{\partial x} = \frac{1}{f_i} (q_i - q_{i+1}) \quad (2)$$

$$\begin{aligned} \rho_i \frac{\partial c_i}{\partial t} + \rho_i c_i \frac{\partial c_i}{\partial x} + \frac{q_{i+1}}{f_i} (c_{i+1} - c_i) \\ + K' \rho_i c_i^2 - K'' \rho_i (U - c_i)^2 = - \frac{\partial P_i}{\partial x} \end{aligned} \quad (3)$$

$$K' = \frac{\lambda' L'}{2f_i} \operatorname{sign} c_i, \quad K'' = \frac{\lambda'' L''}{2f_i} \operatorname{sign} (U - c_i) \quad (4)$$

$$\lambda' = \operatorname{fn}(Re'), \quad \lambda'' = \operatorname{fn}(Re'') \quad (5)$$

$$Re' = \frac{c_i h_i}{2\nu}, \quad Re'' = \frac{(U - c_i) h_i}{2\nu}$$

$$P_i = \rho_i RT \quad (6)$$

The analytical solution to the above set of equations is simplified by defining an equivalent clearance change (ref.12)

$$y_{(e)} = (1 + \xi_i) y_i \quad (7)$$

$$\text{where } \xi_i = \frac{\bar{\delta}_i (\Delta\mu_2 - \Delta\mu_1)}{2 \bar{\mu}_i y_i} \quad (8)$$

Subsequently giving a pressure distribution

$$p_i(\theta) - \bar{p}_i = - \frac{\dot{D}r_i^2}{f_i} \cos \theta + \frac{\bar{c} Dr_i}{f_i} \sin \theta - 2 \left[K'c + K''(U - \bar{c}) \right] \frac{Dr_i^2 \cos \theta}{f_i} \quad (9)$$

$$\text{where } D = \frac{q^*}{2\pi r_i} \left[\frac{Y(e)_{i+1}}{\bar{\delta}_{i+1}} - \frac{Y(e)_i}{\bar{\delta}_i} \right] \quad (10)$$

A possible alternative approach is to apply modified bearing theory to labyrinth chambers. Pinkus and Etison (ref.17) has shown that the Reynolds Equation in a modified form can be used for finite cylinders rotating within moderate clearance ratios, say between 10^{-3} to 10^{-1} which cover likely values for labyrinths.

ADDITIONAL MATERIAL PRESENTED AT THE WORKSHOP

All experimental data presented in figures 6-17 are for straight through seals with mean radial clearance 0.635mm, axial pitch 9.525mm and labyrinth depth 9.525mm. Figure 6 shows the pressure reduction as the working fluid is throttled for a concentric rotor. The resulting circumferential pressure distributions are shown in Figure 7. The expected unbiased pressure distributions are obtained except for slight deviation in chambers 6 and 7. This indicates that any biased pressure profiles would be due to eccentricity, speed or other experimental parameters and can be taken as significant.

Figures 8-11 give the circumferential pressure distribution down the stages for cases of parallel eccentricities; $\epsilon = 0.4, 0.6$ and $u = 94.3, 37.7, 0$ m/s. A restoring force type of pressure distribution with a slight trough is observed in the first chamber. However subsequent chambers give a distribution with minimum pressure just before the minimum gap. These give rise to radial negative spring forces. The profiles are similar in form but with values scaling up with increased eccentricity. Apparently peripheral speeds do not affect the distributions except for the first chamber where the trough increases with speed. Figure 12 shows the pressure ratio for all chambers on an absolute scale for a case seen earlier $\epsilon = 0.6, 94.3$ m/s. It is pointed out here that the experimental points are averaged values of readings taken continuously for each pressure measurement. Scatter are within $\pm 2\%$ and extremely good repeatability is obtained. It is obvious here that unequal pressure field does exist for parallel eccentricity cases. The obtaining of pressure profiles beyond the first chamber shows the limitation of the 'equivalent clearance' pressure prediction of Kurohashi which gives a zero differential pressure field beyond the first chamber.

If the pressure distributions are numerically integrated as defined in the sign convention, figure 13, radial and transverse forces can be obtained. Note that with the sign convention adopted a positive F_y indicates a negative spring force.

Figure 14 gives the radial and transverse forces in individual labyrinth chambers for $u = 94.3$ m/s and $\epsilon = 0.4, 0.6$. The first chamber has a restoring radial force, and beyond this chamber negative spring forces are evident in all stages. These radial forces vary with stage number and eccentricity in a consistent manner, in particular an axial wave variation is clearly present. The transverse force tends to be small and fairly insensitive to eccentricities.

The pressure distributions, as seen earlier, are fairly insensitive to speed and obviously so would the resulting forces, figure 15. Figure 16 gives the radial and transverse forces for several eccentricities. The radial forces are dependent on eccentricity and the transverse forces much less so. Figure 17 gives the summation of radial and transverse forces plotted against eccentricity, with the linear relationship of F_y with eccentricity seen.

The above results presented are some of the experiments done with the recent commissioning of the test rig. Obviously the full experimental schedule is yet to be undertaken and it is hopeful that meaningful results will be obtained. The effects of these forces will be incorporated into a model of a real rotor using the rotordynamic computer programme of the Department in the near future.

REFERENCES

1. Pollman, E., Schwerdtfeger, H. and Termuehlen, H.: Flow Excited Vibrations in High Pressure Turbines (Steam Whirl). Trans. ASME, J.Engng. Power, April 1978, pp. 219-228.
2. Alford, J.S.: Protecting Turbomachinery from Self-Excited Rotor Whirl. Trans. ASME, J. Engng. Power, October 1965, pp. 333-344.
3. Spurk, J.H. and Keiper, R.: Self-Excited Vibration in Turbomachines resulting from Flow through Labyrinth Glands. C.E. Trans. 6785. Translated from Ingenieur Archiv. Vol. 43 (1974), pp. 127-135.
4. Greathead, S.H. and Bastow, P.: Investigations into Load Dependent Vibrations of the High Pressure Rotor on Large Turbo-Generators. I.Mech.E. Conference on Vibrations in Rotating Machinery. September 1976.
5. Greathead, S.H. and Slocombe, M.D.: Further Investigations into Load Dependent Low Frequency Vibration of the High Pressure Rotor on Large Turbo-Generators. I.Mech.E. Conference on Vibrations in Rotating Machinery, September 1980.
6. Den Hartog, J.P.: Mechanical Vibrations, McGraw-Hill Book Co. Inc., New York, fourth edition, pp. 295- 296.
7. Thomas, H.J.: Unstable Oscillations of Turbine Rotors due to Steam Leakage in the Clearances of the Sealing Glands and Blading, C.E. Trans. 6281. Translated from A.I.M. Bull. Sci. (1958) Vol. 71, Nos. 11, 12.
8. Rosenberg, C.S., Orlik, W.G. and Marshenko, U.A.: Investigating Aerodynamic Transverse Forces in Labyrinth Seals in Cases Involving Rotor Eccentricity. C.E. Trans. 7083. Translated from Energomashinostrojenie Vol. 8, 1974, pp. 15-17.

9. Orlik, W.G., et al: The Centring Effect in Labyrinth Type Seals and its Effect on Low Frequency Vibration of Turbo-Machines. C.E. Trans. 7104. Translated from Energomashinostrojenie Vol. 10, 1975, pp. 25-29.
10. Kostyuk, A.G.: A Theoretical Analysis of the Aerodynamic Forces in the Labyrinth Glands of Turbomachines. Thermal Engineering Vol. 19 1972 (11), pp. 39-44 (Teploenergetika 1972, 19 (11) pp. 29-33).
11. Iwatsubo, T.: Evaluation of the Instability Forces of Labyrinth Seals in Turbines or Compressors. Symposium - Workshop on Rotordynamic Instability Problems in High-Performance Turbomachinery. Texas A&M Univ., May 1980. NASA Conference Publication 2133.
12. Kurohashi, M., Inoue, Y., Abe, T. and Fujikawa, T.: Spring and Damping Coefficients of the Labyrinth Seals. I, Mech.E. Conference on Vibrations in Rotating Machinery. September 1980.
13. Benckert, H. and Wachter, J.: Investigations on the Mass Flow Induced Forces in Contactless Seals of Turbomachines. Proceedings of the 6th Conference on Fluid Machinery, Budapest 1979, pp. 57-66.
14. Benckert, H. and Wachter, J.: Flow Induced Coefficients of Labyrinth Seals for Application in Rotordynamics. Symposium - Workshop on Rotordynamic Instability Problems in High Performance Turbomachinery, Texas A&M Univ., May 1980, NASA Conference Publication 2133.
15. Benckert, H. and Wachter, J.: Flow Induced Constants of Labyrinth Seals. I. Mech.E. Conference on Vibrations in Rotating Machinery, September 1980.
16. Vermes, G.: A Fluid Mechanics Approach to the Labyrinth Seal Leakage Problem. Trans. ASME, J. Engng. Power, April 1961, pp. 161-169.
17. Pinkus, O. and Etsion, I.: Analysis of Finite Cylinders Rotating Within Moderate Clearance Ratios. Trans. ASME, J. Fluids Engng., June 1976, pp. 156-162.

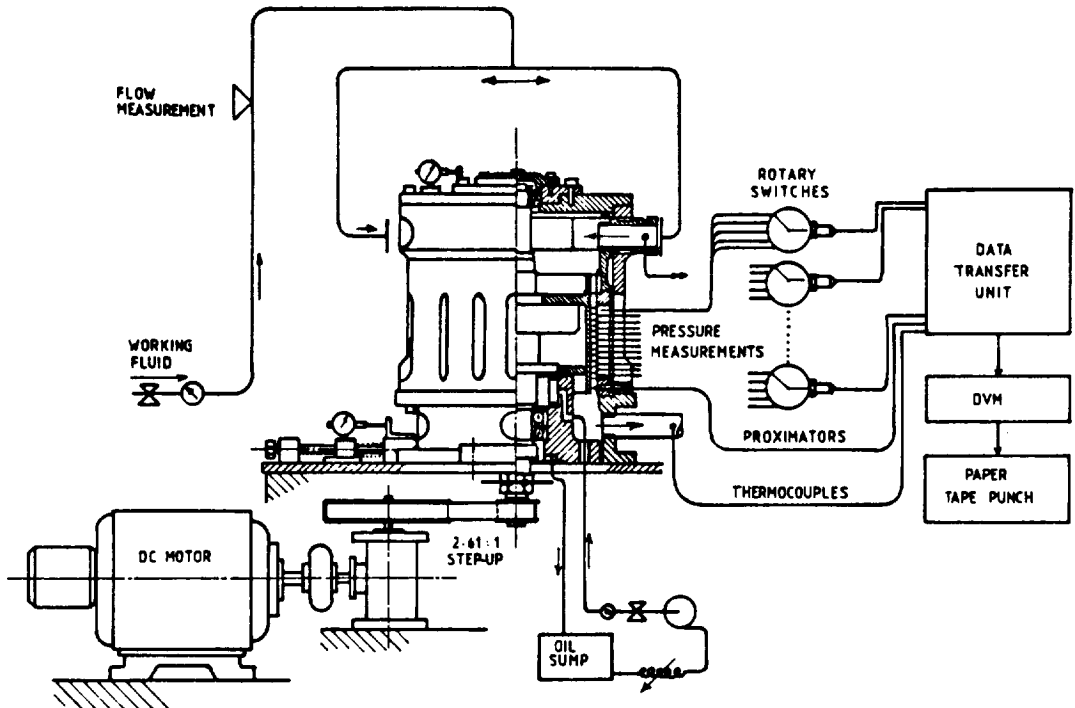


Figure 1. - Schematic layout of test rig and instrumentations.

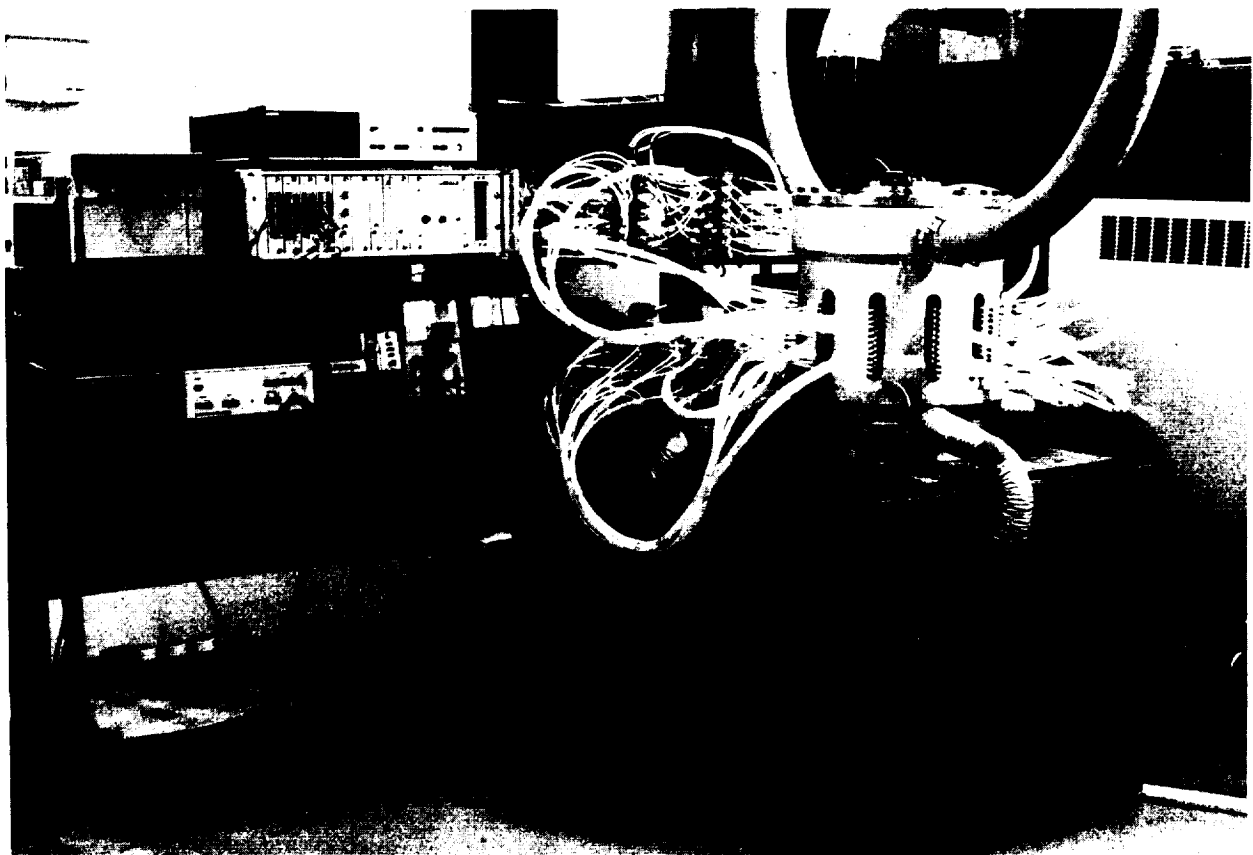
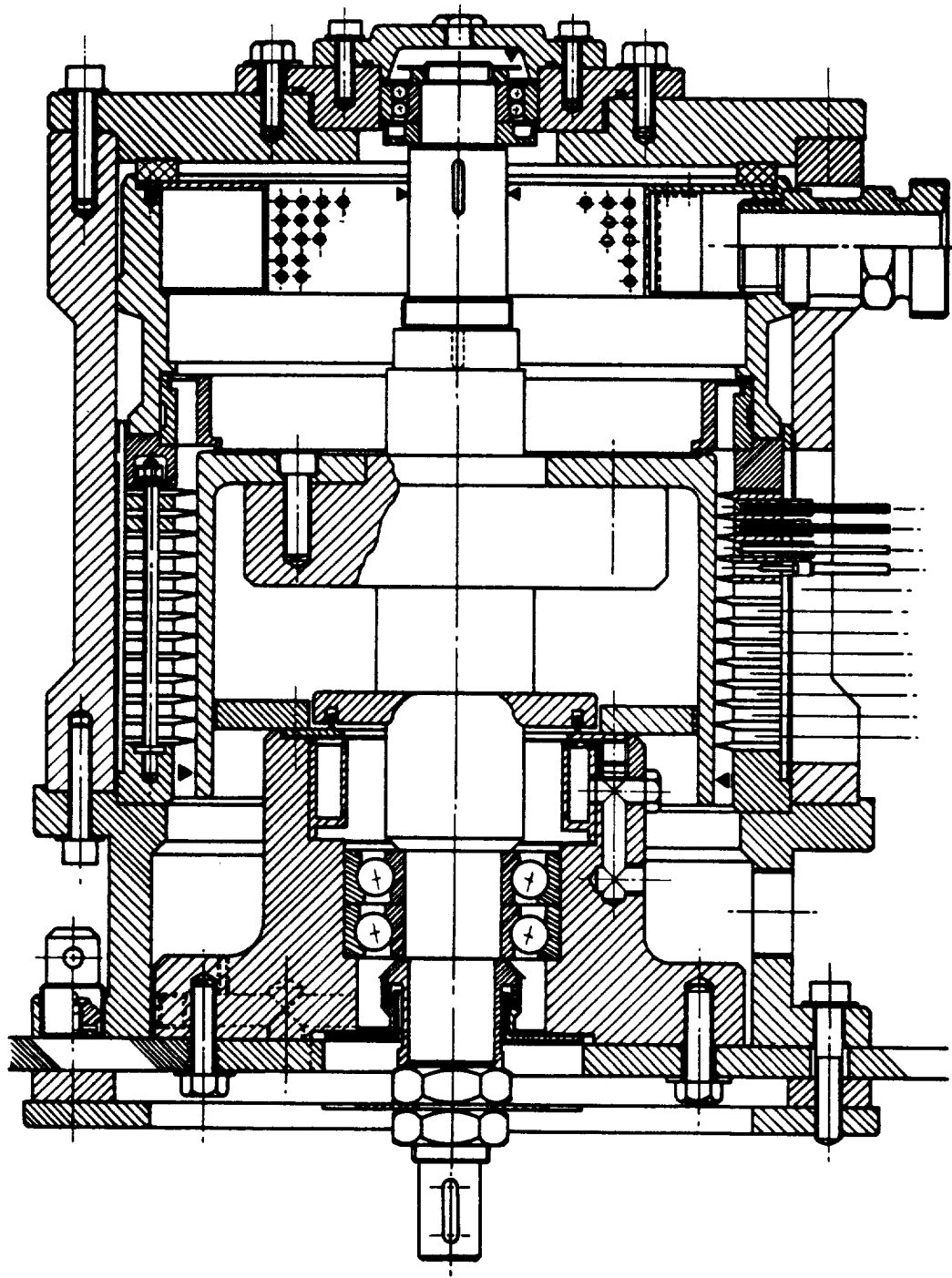
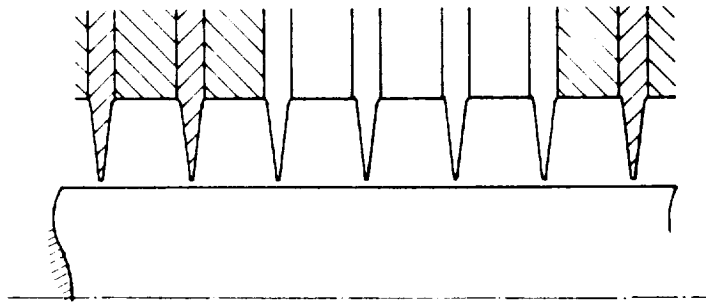


Figure 2. - View of overall test rig.

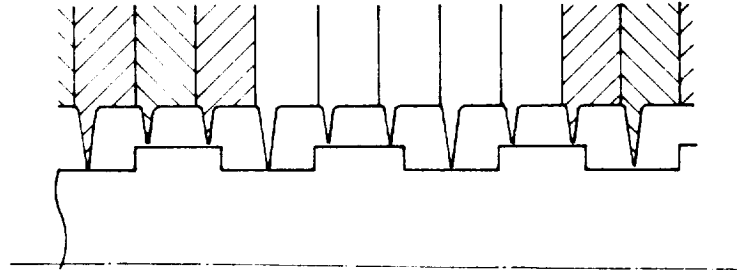


0 50 100 mm

Figure 3. - Sectioned assembly drawing of test rig (main assembly).



(a). - Straight through labyrinths.



(b). - Combination labyrinths.

Figure 4. - Types of built-up labyrinth stack.

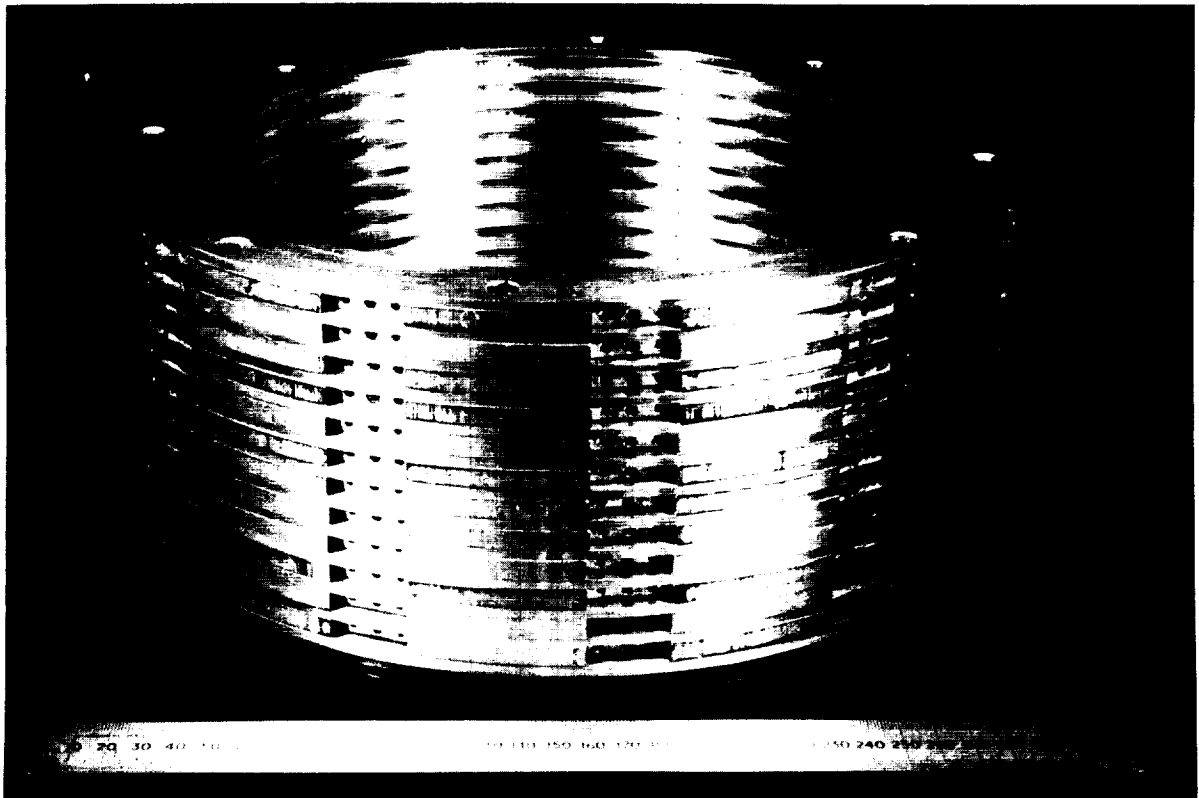


Figure 5. - View of built-up straight through labyrinths.

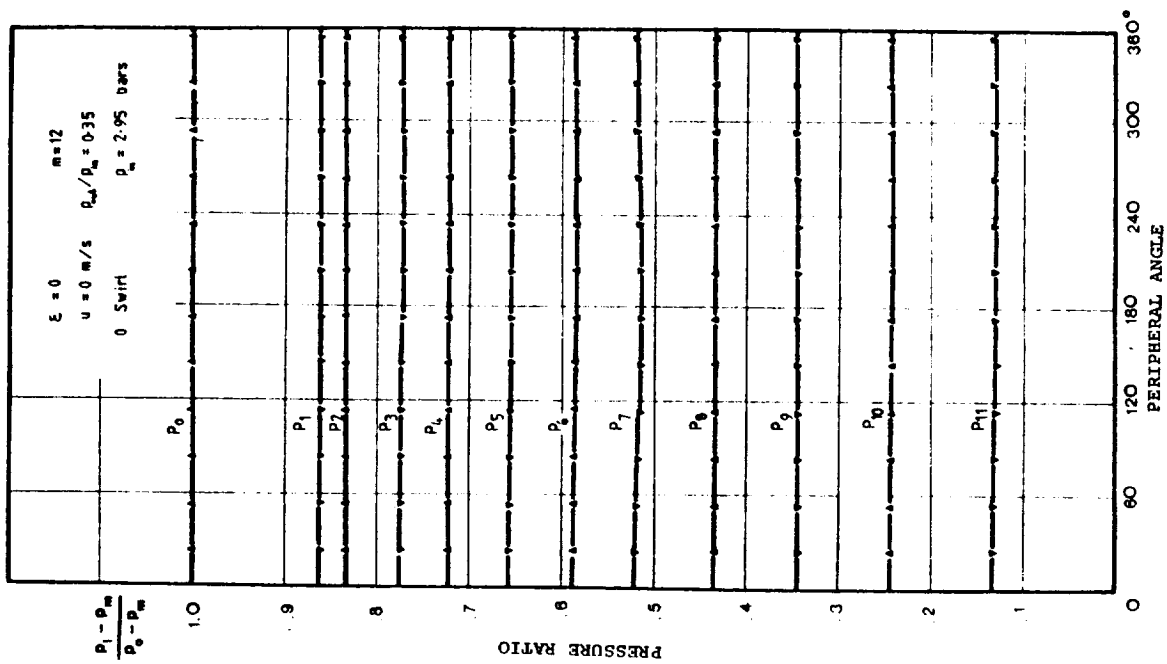


Figure 7. - Pressure distribution, concentric rotor.

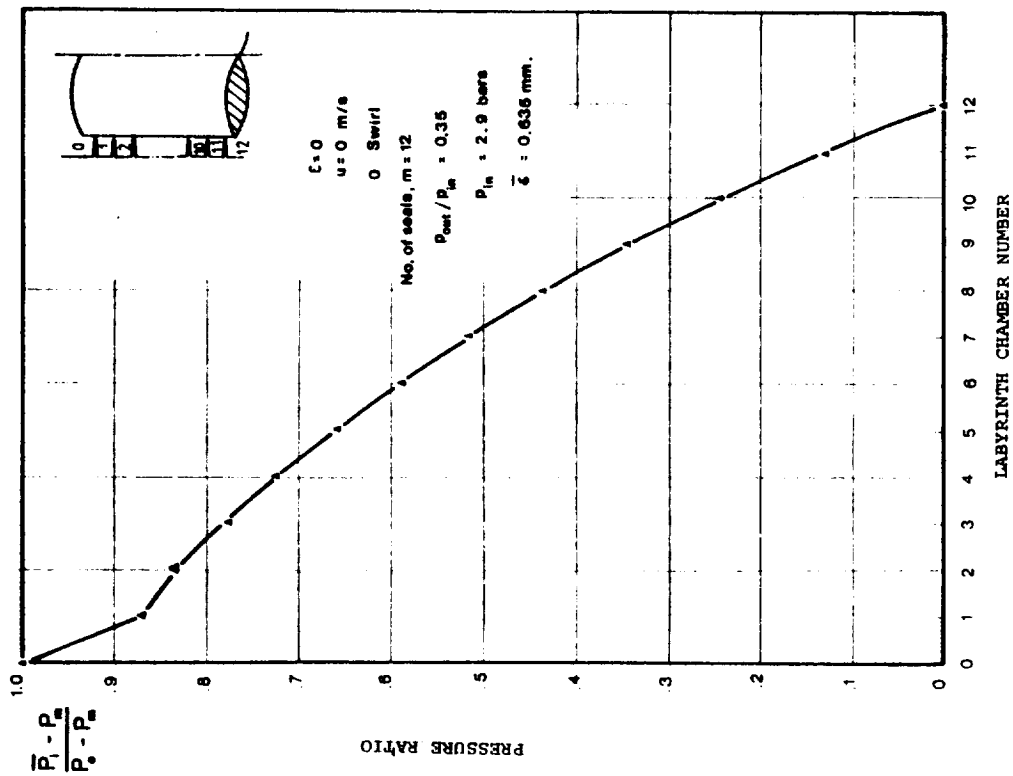


Figure 6. - Pressure expansion through the stages, concentric rotor

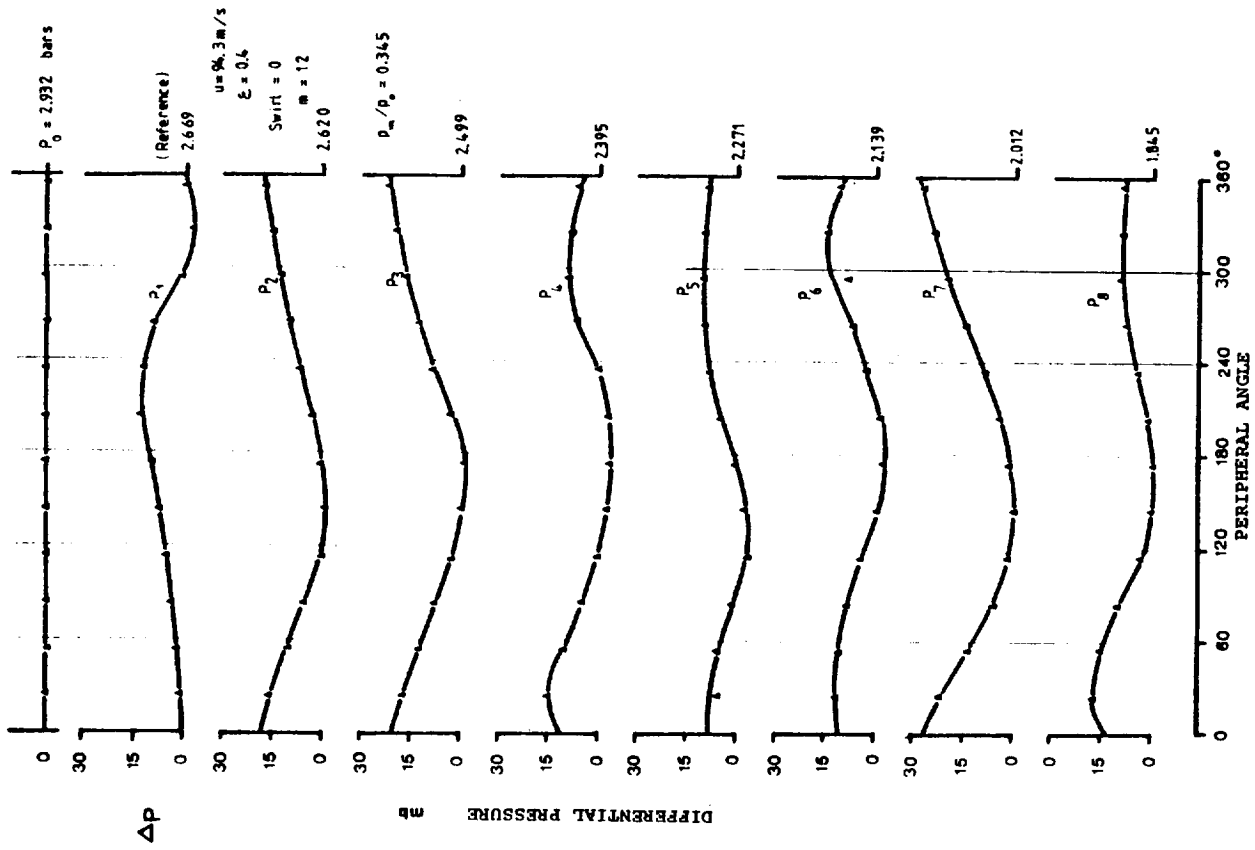


Figure 8. - Pressure distribution, parallel eccentricity.

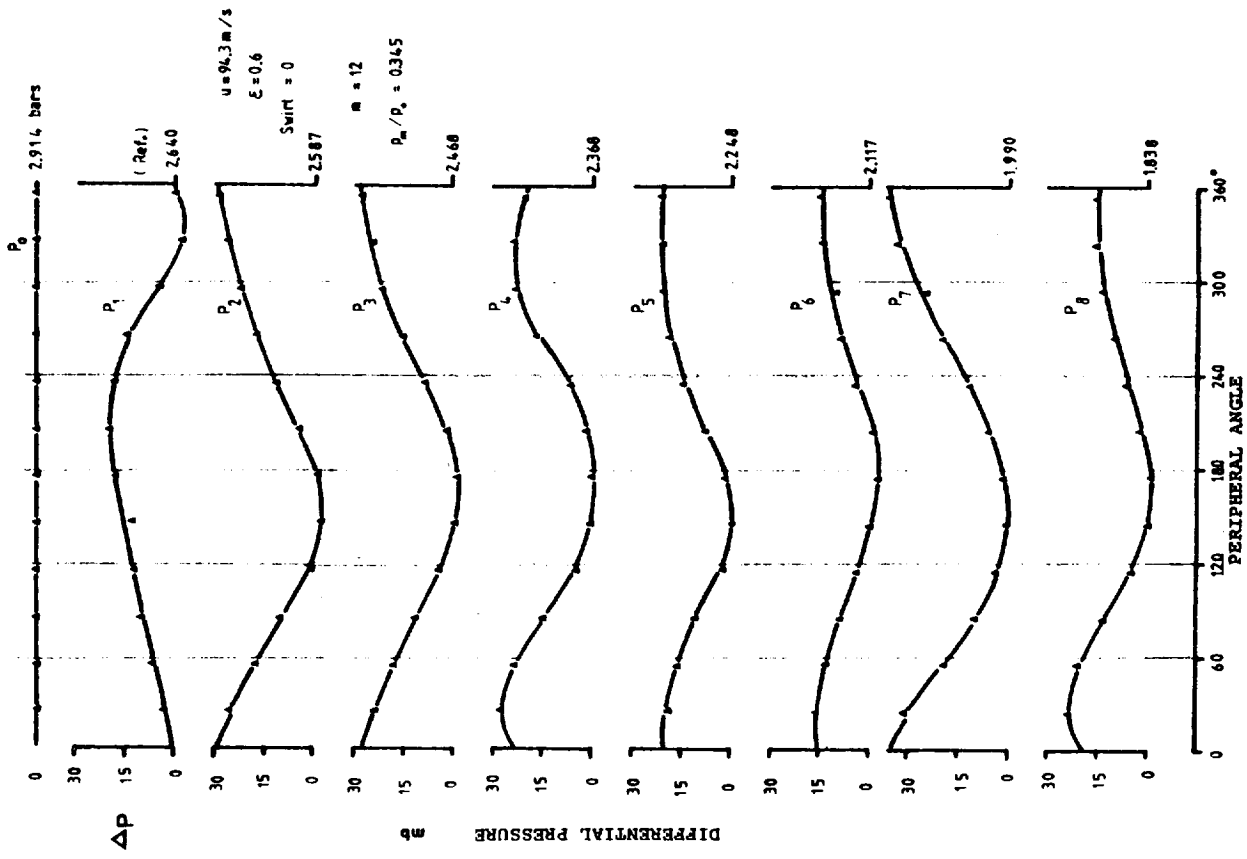


Figure 9. - Pressure distribution, parallel eccentricity.

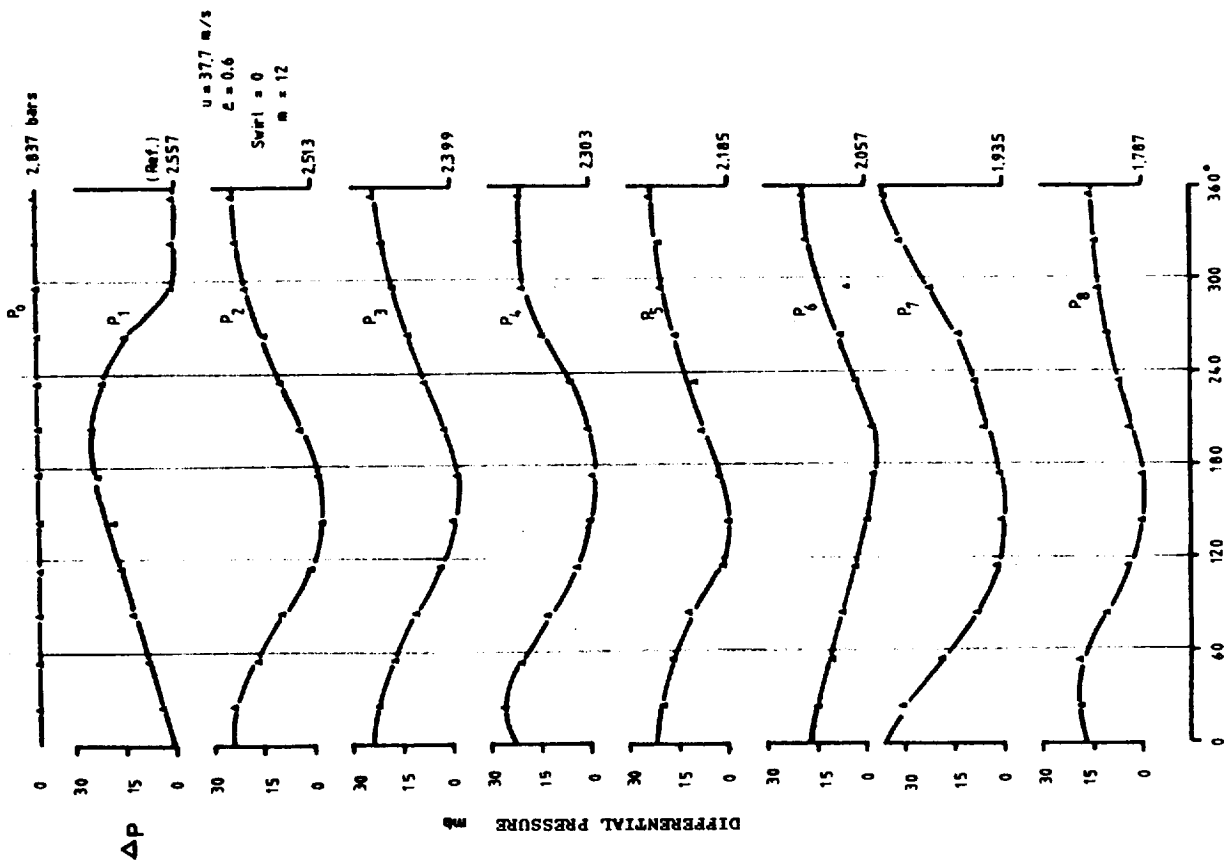


Figure 10. - Pressure distribution, parallel eccentricity.

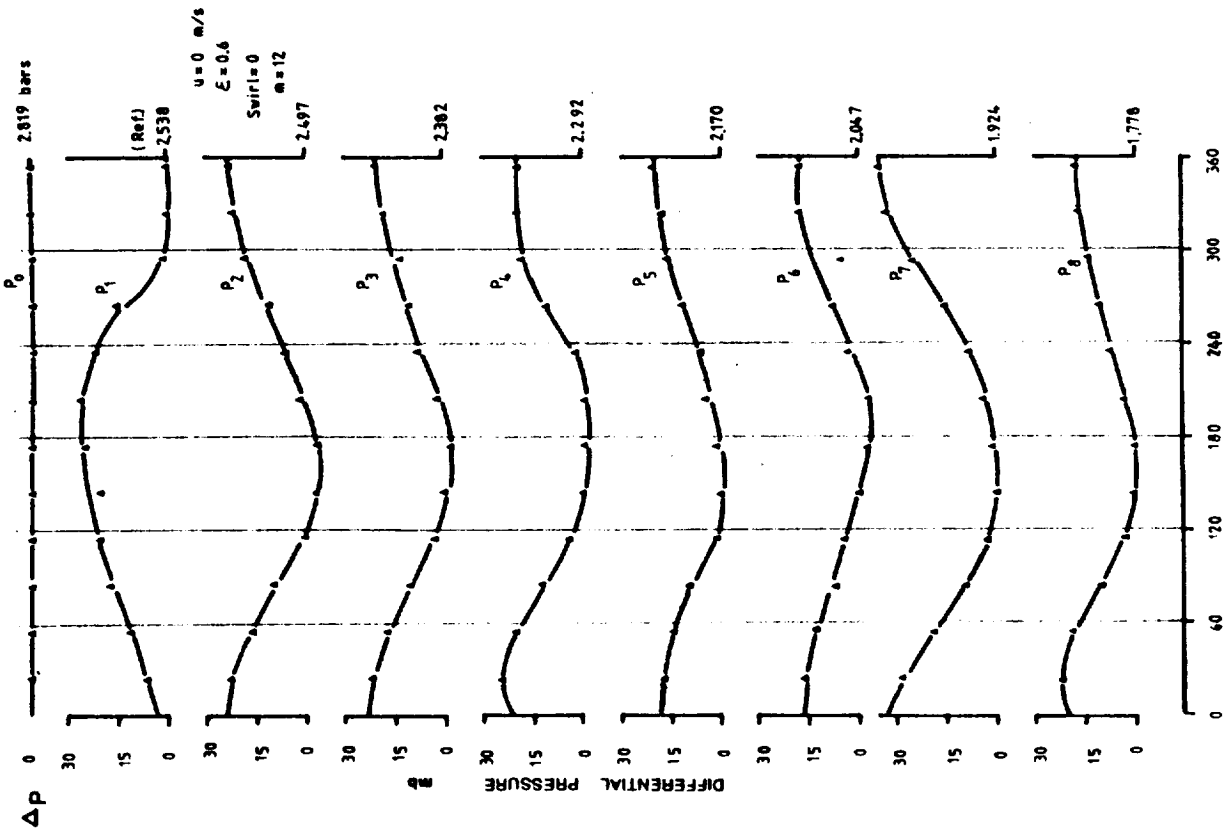


Figure 11. - Pressure distribution, parallel eccentricity.

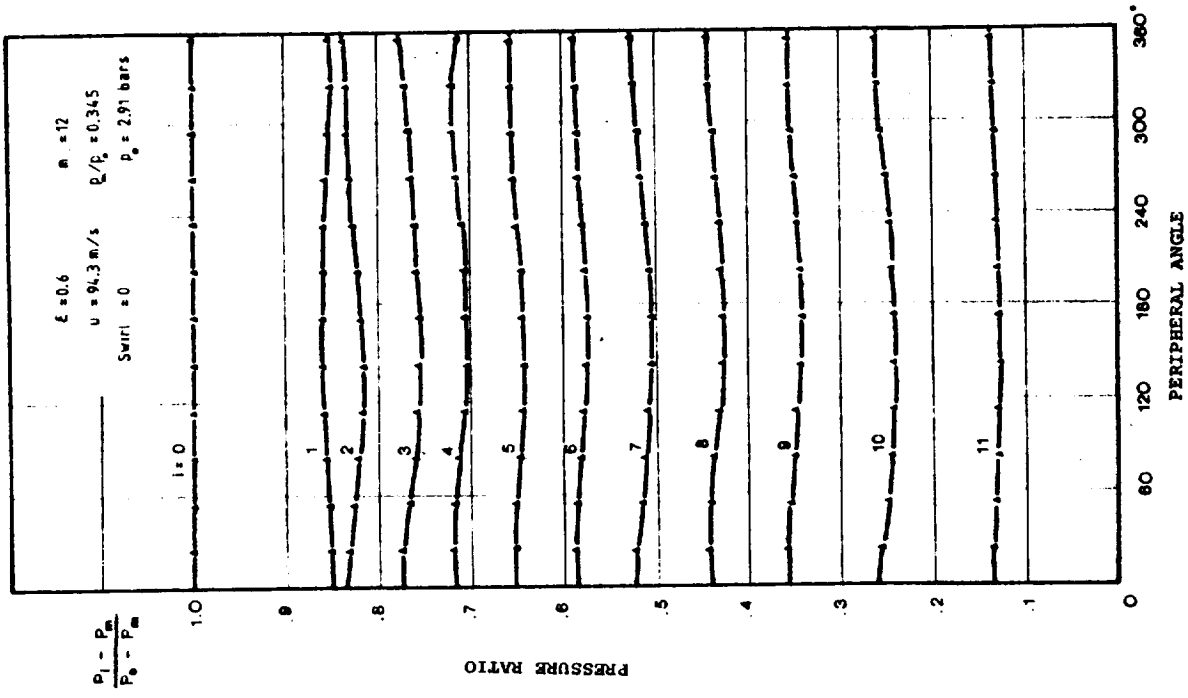
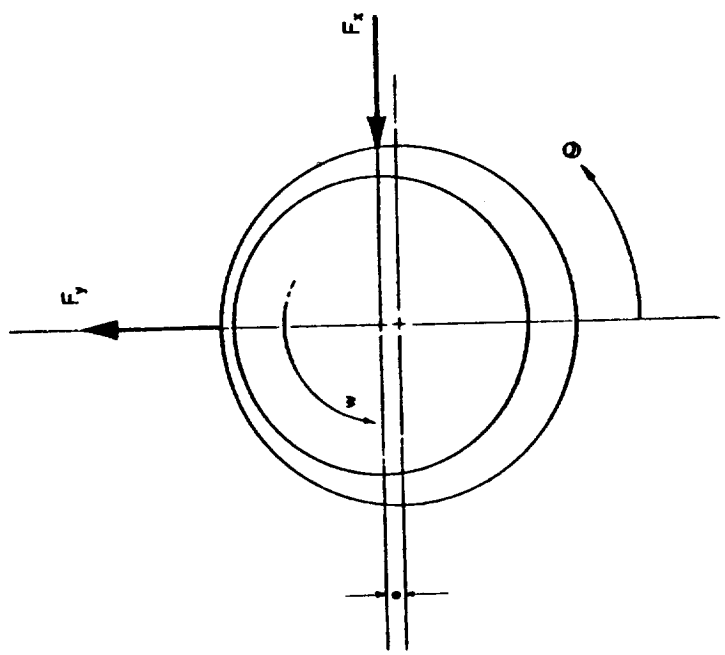


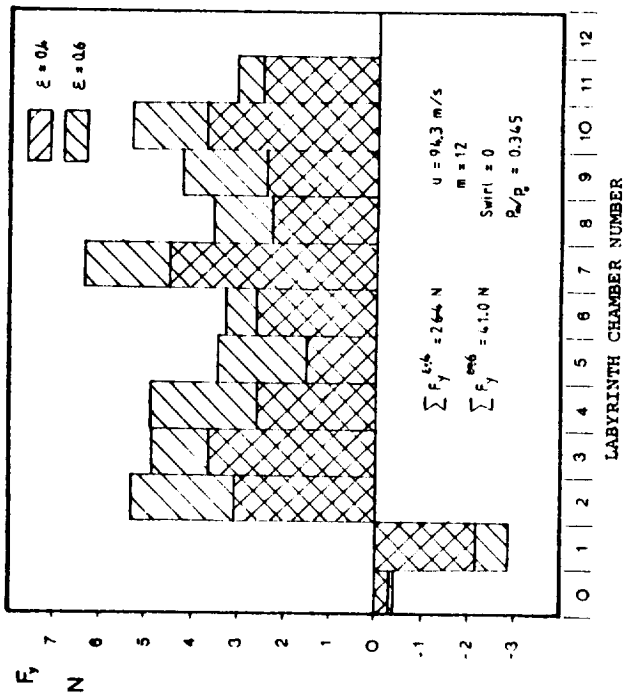
Figure 12.



$$F_y = \int_0^{2\pi} r L p \cos \theta \, d\theta$$

$$F_x = \int_0^{2\pi} r L p \sin \theta \, d\theta$$

Figure 13.-- Sign convention for eccentricity and forces.



RADIAL FORCE IN INDIVIDUAL LABYRINTH CHAMBER

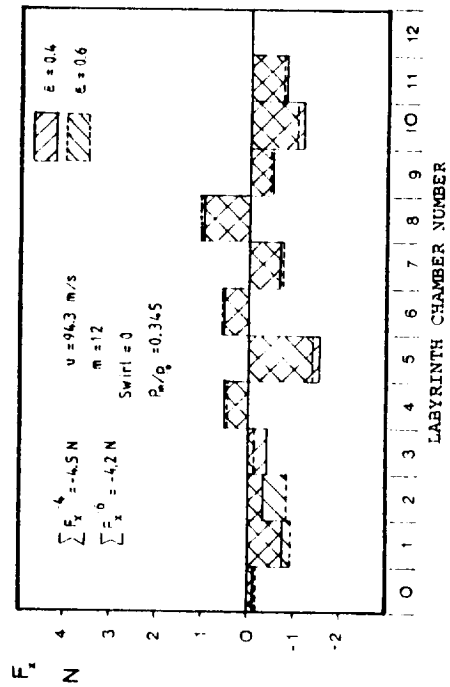


Figure 14. - Transverse force in individual labyrinth chamber.

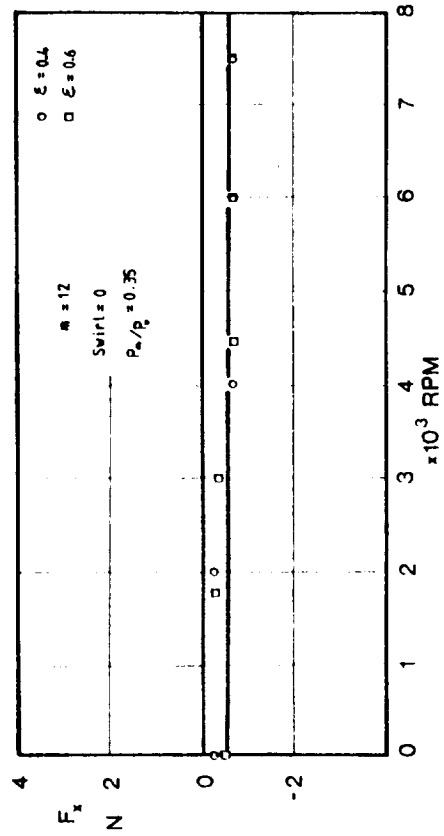
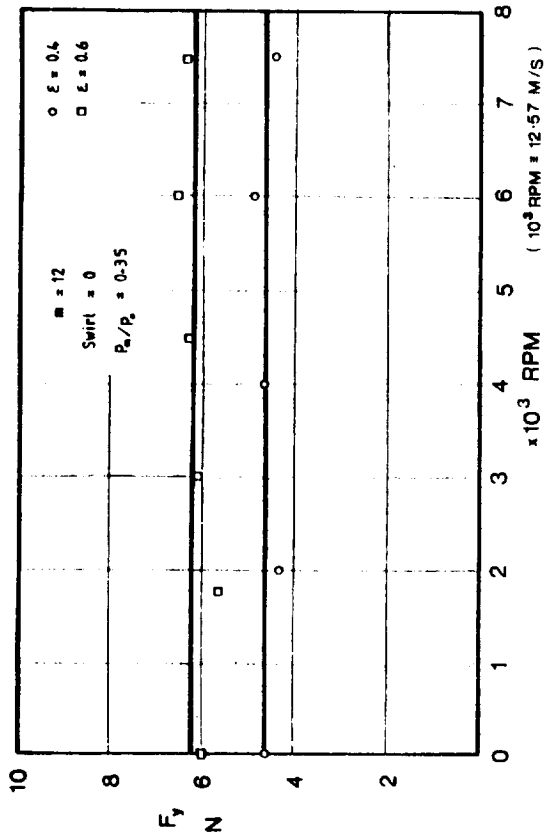
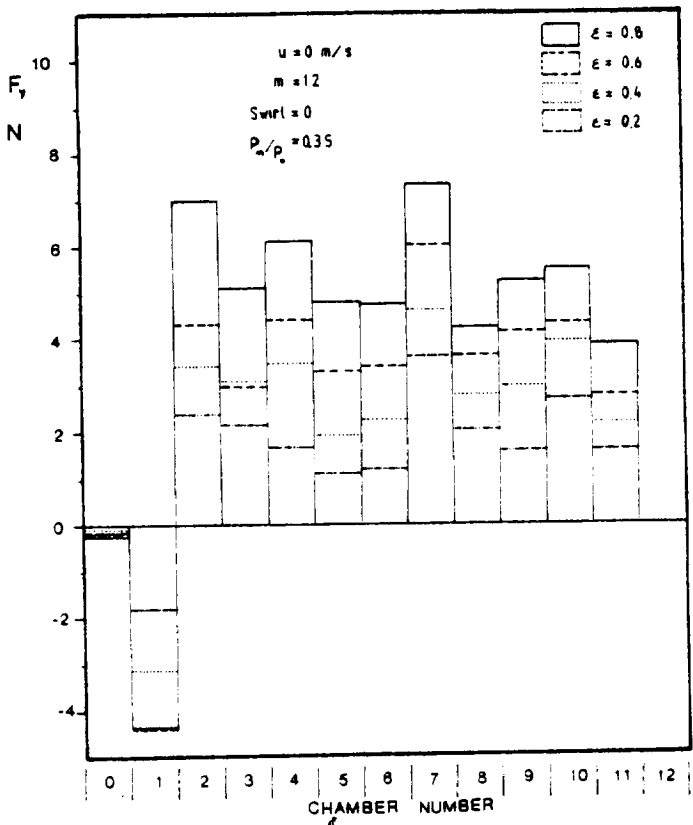
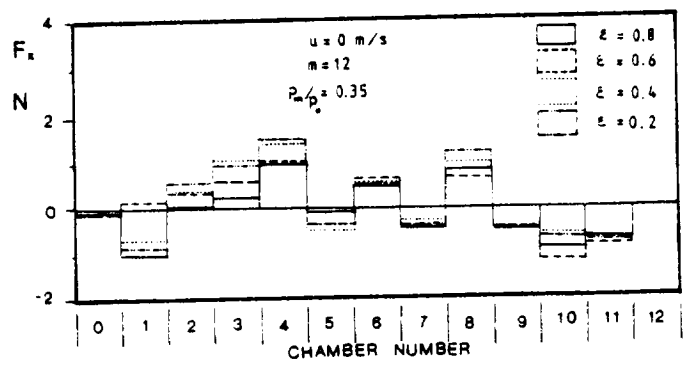


Figure 15. - F_y , F_x in typical chamber (chamber 7) versus speed.



(a). - Radial force.



(b). - Transverse force.

Figure 16. - Radial and transverse forces in individual labyrinth chamber.

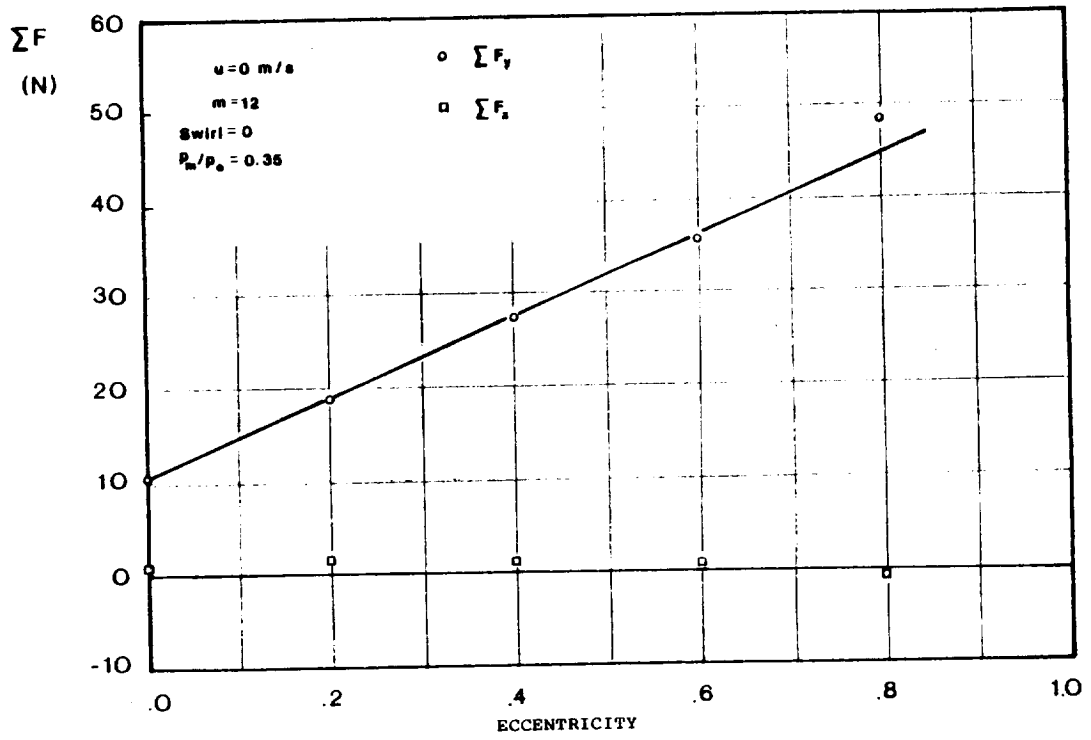


Figure 17. - ΣF_y , ΣF_x vs. eccentricity.